Ocean Engineering ▮ (▮▮▮▮) ▮▮▮–▮▮▮

Contents lists available at ScienceDirect

Ocean Engineering

journal homepage: www.elsevier.com/locate/oceaneng

A seakeeping analysis method for an air-lifted vessel

Nan Xie, D. Vassalos, A. Jasionowski, P. Sayer *

Department of Naval Architecture and Marine Engineering, Universities of Glasgow and Strathclyde, Henry Dyer Building, 100 Montrose Street, Glasgow G4 0LZ, UK

ARTICLE INFO

Article history:
Received 14 October 2007
Accepted 12 June 2008

Keywords:
Seakeeping
Frequency domain
Air-lifted vessel
Numerical prediction

ABSTRACT

A seakeeping analysis in the frequency domain is presented to predict the motion response of an air-lifted vessel (ALV) in waves. The ALV is supported by pressurised air in two separate cushion chambers; the pressure variation in the cushions has a significant effect on the motions of the vessel. The adiabatic gas law is used to couple cushion pressure and the free-surface elevation of water inside the chamber. Attention is focused on the waves generated by the pressure, and a method is presented to compute the corresponding free-surface elevation. New numerical schemes are proposed for calculating the three-dimensional free-surface elevation for the four wave numbers. Numerical results of the free-surface elevation, escape area, escape volume and motion responses of the ALV are provided.

1. Introduction

The innovative design of an air-lifted vessel (ALV) utilises the cushioning and lubricating properties of air to generate an efficient high-speed marine vehicle. An energy saving of up to 25% is possible compared to conventional high-speed mono-hulls or catamarans, based on model experiments by Allenstrom et al. (2001, 2003).

The selected ALV is a skirtless SES catamaran. There are two demi-hulls, each of which contain an air cushion (see Fig. 1). The design feature of the ALV is similar, in some sense, to that of an SES catamaran. There are two demi-hulls, each of which contains air cushions. A forward planing surface ahead of the step creates some limited dynamic lift. The step and the forward planing surface also create the forward ceiling of the air cushion chamber, the step being located in a plane close to horizontal (no part of the step is to ventilate before the other). The bow section is slender in order to reduce displacement forces in a seaway, and the bow incorporate a voluminous part above a built-in chine/spray rail to reduce water deflection and reserve buoyancy in pitching motion. The side keels of varying height extend from just ahead of the step to the transom. The height of the keels is adjusted to the observed/expected shape of the air cushion. The only purpose of the side keels is to fence in the air cushion. There are spray rails on the outside of the side keels, at a height partly to deflect the water without wetting the rails on the upper sides. The cushion ceiling is at a height to avoid being hit by waves when the vessel is moving. The ceiling aft end slopes to deflect passing waves. A flap or enclosure arrangement in line with the sloped portion of the ceiling is positioned to 'fence' the air cushion chamber in the rear part and to create dynamic lift and motion damping. The air cushion concept of the present ALV is patented (EFFISES Project, 2001–2004). More details about the ALV concept can be found in Allenstrom et al. (2001).

In the 'on-cushion' mode, the vessel is mainly supported by the difference between the ambient atmospheric pressure and that in the plenum chamber. The pressure of the air captured in the chamber undergoes a pressure variation, and thus waves are generated on the free-surface. The dynamic response of the ALV in turn causes a reaction on the craft through the captured air, which generates further variation of the air pressure. The motions affect passenger and crew comfort as well as the performance of electronic components and machinery on board. In the present paper, a method is presented for the numerical prediction of the seakeeping performance of the ALV; this is similar to that for a surface-effect ship (SES), previously studied by other researchers, including Doctors (1976), Chen (1977), Kim and Tsakonas (1981), Kaplan et al. (1981), and Faltinsen (2005).

As the ALV is supported by pressurised air in two separate cushion chambers, the behaviour of the craft in waves is mainly due to the pressure variation in the cushion chambers. The adiabatic gas law is used to couple cushion pressure and the free-surface elevation inside the chambers. Computations of the corresponding wave patterns are presented. Efficient and effective numerical schemes are proposed for calculating the three-dimensional free-surface elevation for the four wave numbers. Numerical results are also presented for the free-surface elevation, air cushion escape area and escape volume, and for the motion of the vessel in irregular waves.

2. Equations of motion of the ALV

A right-handed coordinate system *oxyz* is adopted with the plane $z = 0$ in the undisturbed free-surface and z positive

* Corresponding author. Tel.: +44 141 548 3302; fax: +44 141 552 2879.
E-mail address: p.g.sayer@na-me.ac.uk (P. Sayer).

0029-8018/$ - see front matter © 2008 Elsevier Ltd. All rights reserved.
doi:10.1016/j.oceaneng.2008.06.011

Nomenclature

a	length of a rectangular pressure patch
$a_{i,j}$	$i, j = 3, 4, 5$, added mass for pitch, heave and roll
A	parameter of wave spectra
A_c	cushion area
A_L	escape area
A_{L0}	outflow opening area at equilibrium condition
A_{LW}	cushion opening area due to incident wave
b	beam of a rectangular pressure patch
$b_{i,j}$	$i, j = 3, 4, 5$, damping for pitch, heave and roll
B	parameter of wave spectra
b_{pi}	$i = 3, 5$ coefficients for pressure and motion coupling equation
b_{pp}	coefficient for pressure and motion coupling equation
B_T	width of outflow opening
c_n	flow coefficient
$c_{i,j}$	$i, j = 3, 4, 5$, hydrostatic restoring coefficients for pitch, heave and roll
c_{pi}	$i = 3, 5$ coefficients for pressure and motion coupling equation
c_{pp}	coefficient for pressure and motion coupling equation
E_1	exponential integral
f_m	$m = 1, 2, \ldots, 8$, function
Fn	length Froude number of a pressure patch
$\mathbf{F}_H$	hydrodynamic force/moment vector
$\mathbf{F}_R$	hydrostatic force/moment vector
$\mathbf{F}_P$	force/moment vector due to cushion pressure
$\mathbf{F}_W$	wave exciting force/moment vector
F_{wj}	$j = 3, 4, 5$, wave exciting force/moments
F_{wp}	right-hand side term in the pressure and motion coupling equation
g	acceleration due to gravity
g_m	function
$H_{1/3}$	significant wave height
I_{ij}	$j = 4, 5$, craft mass inertia moment for roll and pitch
J_{im}	$i = 0, 1, \ldots, 6$, $m = 1, 2, \ldots, 8$, terms in the wave elevation for a rectangular pressure patch
k_i	$i = 0, 1, 2, 3, 4$, wave numbers
L	craft length
m	index
$\mathbf{M}$	mass/inertia matrix
p	cushion pressure
p_a	atmospheric pressure
p_i	pressure in cushion chambers
p_0	pressure in cushion chamber at equilibrium condition
$\mathbf{q}$	craft motion responses
q_{ka}	amplitudes of motion response
Q_{in}	inflow rate
Q_{out}	outflow rate
RMS	root mean square of the motion responses
S_{jk}	$j, k = 0, 1$, moments of cushion area
s_m	$m = 1, 2, \ldots, 8$, variables for wave elevation of rectangular pressure patch
S_ς	wave spectrum
T_{01}	average wave period
u	variable of functions
U	craft speed
V	cushion volume
v_p	escape volume
v_w	cushion pumping volume due to incident wave
$\tilde{v}_p$	non-dimensional escape volume
x, y, z	coordinates
x_c, y_c	centre of cushion area
z	heave
Z	height of cushion ceiling
α	escape area
$\tilde{\alpha}$	non-dimensional area
α_p	escape area due to cushion pressure
γ	ratio of specific heats for gas, Euler's constant; also a parameter in the wave elevation integrals
ϕ	roll motion of the craft
μ	wave heading
θ	pitch motion; also a general angle
θ_c	cut-off angle
ρ	density
ρ_a	atmospheric air density
ρ_0	density of air at equilibrium condition
ρ_w	water density
σ	encounter frequency
τ	reduced frequency
ς_p	free-surface elevation due to cushion pressure
ς_w	incident wave elevation
ψ	a general function

upwards. The origin is located at C.G. of the vessel. Frequency domain analysis method will be used in the present study. The equation of motions of the ALV can be expressed as

$$[\mathbf{M}][\ddot{\mathbf{q}}] = [\mathbf{F}_H] + [\mathbf{F}_R] + [\mathbf{F}_P] + [\mathbf{F}_W], \tag{1}$$

where $\mathbf{q}$ is the motion vector of the vessel, $\mathbf{M}$ is the mass/inertia matrix, $\mathbf{F}_H$ is the hydrodynamic force/moment, $\mathbf{F}_R$ is the hydrostatic force/moment, $\mathbf{F}_P$ is the force/moment due to the cushion pressure, and $\mathbf{F}_W$ is the wave exciting force/moment.

The adiabatic gas law and continuity equation for the air in each chamber are used to determine the cushion pressure in the port and starboard chambers:

$$\begin{cases} \dfrac{p_i + p_a + p_{0,i}}{\rho_i^{\gamma}} = \text{constant}, \\ V_i \dfrac{d\rho_i}{dt} + \rho_i \dfrac{dV_i}{dt} = \rho_a Q_{in,i} - \rho_a Q_{out,i}, \end{cases} \tag{2}$$

where the subscripts $i(=1,2)$ denote the port and starboard cushions, respectively; henceforth, for clarity this subscript will be omitted unless specifically required; p_0 and ρ_0 are cushion pressure and air density at equilibrium operating condition; p_a and ρ_a are atmospheric pressure and air density; Q_{in} and Q_{out} are the inflow and out flow rate; V is the cushion volume, determined by vessel motion attitude, incident wave and cushion pressure:

$$V = \iint_{A_c} [Z(x,y) - \varsigma_p(x,y) - \varsigma_w(x,y)]\, dx\, dy \tag{3}$$

where Z is the cushion ceiling height, ς_w and ς_p are incident wave and free-surface elevation due to cushion pressure, respectively. The outflow rate can be expressed as

$$Q_{out} = c_n A_L \sqrt{\frac{2(p + p_0)}{\rho_a}} \tag{4}$$

where $c_n(\approx 0.6-0.8)$ is the flow coefficient and A_L is the air escape area of the flow opening at the cushion stern boundary:

$$A_L = \int_{y_a}^{y_b} [Z(x_T, y) - \varsigma_p(x_T, y) - \varsigma_w(x_T, y)]\, dy \tag{5}$$

where x_T is the longitudinal coordinate of cushion stern aperture.

Please cite this article as: Xie, N., et al., A seakeeping analysis method for an air-lifted vessel. Ocean Engineering (2008), doi:10.1016/j.oceaneng.2008.06.011

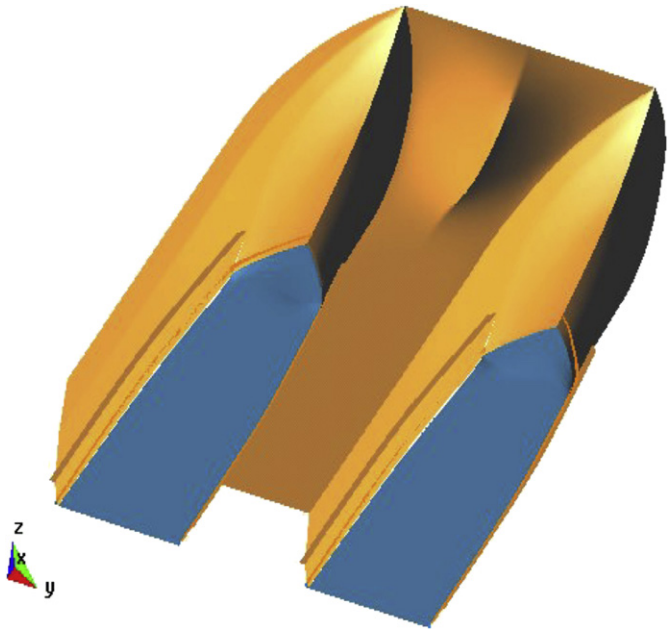

Fig. 1. The ALV concept.

Expanding (2) about the vessel's equilibrium position, and assuming small amplitudes of motion for the ALV, the linearised cushion pressure equation can be written as

$$b_{pp}\dot{p} + c_{pp}p + b_{p3}\dot{z} + c_{p3}z + b_{p5}\dot{\theta} + c_{p5}\theta + b_{p4}\dot{\phi} + c_{p4}\phi = F_{wp} \tag{6}$$

where

$$b_{pp} = \frac{V_0\rho_0^{1+\gamma}}{\gamma p_0} - \rho_0 v_p \tag{7}$$

$$c_{pp} = \rho_a\left|\frac{\partial Q_{in}}{\partial p}\right|_0 + c_n\frac{\rho_a A_{L0}}{\sqrt{2p_0\rho_a}} - c_n\alpha\sqrt{\frac{2p_0}{\rho_a}} \tag{8}$$

$$b_{p3} = -\rho_0 A_c \tag{9}$$

$$c_{p3} = -c_n\rho_a B_T\sqrt{\frac{2p_0}{\rho_a}} \tag{10}$$

$$b_{p5} = \rho_0 x_c A_c \tag{11}$$

$$c_{p5} = c_n\rho_a x_c B_T\sqrt{\frac{2p_0}{\rho_a}} \tag{12}$$

$$b_{p4} = -\rho_0 y_c A_c \tag{13}$$

$$c_{p4} = -c_n\rho_a y_c B_T\sqrt{\frac{2p_0}{\rho_a}} \tag{14}$$

$$F_{wp} = \rho_0\dot{v}_w + c_n A_{Lw}\sqrt{\frac{2p_0}{\rho_a}} \tag{15}$$

In the above, V_0 is the cushion volume at equilibrium condition; (x_c, y_c) is the cushion centre; A_c is the cushion area; $\partial Q_{in}/\partial_p$ is the discharge by fan per unit pressure; v_p and α_p are the escape volume and escape area resulting from unit cushion pressure; z, θ, ϕ are heave, pitch and roll motions; A_{L0} is the outflow opening area at equilibrium condition; B_T is the width of the outflow opening; v_w and A_{Lw} are the cushion pumping volume and opening area, respectively, due to the incident waves:

$$v_w = \iint_{A_c}\varsigma_w(x,y)\,dx\,dy \tag{16}$$

$$A_{Lw} = \int_{y_a}^{y_b}\varsigma_w(x_T,y)\,dy \tag{17}$$

The cushion escape volume and escape area are given, respectively, by

$$v_p = \iint_{A_c}\varsigma_p(x,y;\sigma)\,dx\,dy \tag{18}$$

$$\alpha_p = \int_{y_a}^{y_b}\varsigma_p(x_T,y;\sigma)\,dy \tag{19}$$

Physically, the cushion escape volume is the volume resulting from the free-surface elevation, due to cushion pressure, inside the cushion chamber of the ALV; while the escape area is the area generated by this free-surface profile along the stern opening of the cushion chamber. The equations of heave, pitch and roll may be linearised relative to the equilibrium position of the ALV:

$$\begin{cases}(m+a_{33})\ddot{z}_3 + b_{33}\dot{z} + c_{33}z + a_{35}\ddot{\theta} + b_{35}\dot{\theta} + c_{35}\theta - S_{00}(p_1+p_2) = F_{w3},\\ a_{53}\ddot{z} + b_{53}\dot{z} + c_{53}z + (I_{55}+a_{55})\ddot{\theta} + b_{55}\dot{\theta} + c_{55}\theta + S_{10}(p_1+p_2) = F_{w5},\\ (I_{44}+a_{44})\ddot{\phi} + b_{44}\dot{\phi} + c_{44}\phi - S_{01}(p_1-p_2) = F_{w4},\end{cases} \tag{20}$$

where a_{ij} and b_{ij} are the added mass and damping coefficients of the rigid side-hull, c_{ij} is the hydrostatic restoring coefficient, F_{wj} is the wave exciting force/moment, and

$$S_{jk} = \iint_{A_c}x^j y^k\,dx\,dy \quad j,k = 0,1 \tag{21}$$

are the moments of the cushion area. The hydrodynamic coefficients and wave exciting force/moments on the thin rigid side-hull of each cushion are calculated by strip theory.

Hence, the transfer functions for heave, pitch and roll in regular waves can be obtained. The root mean square (RMS) values are

$$\mathrm{RMS}_k(\mu) = \left(\int_0^\infty\left(\frac{q_{ka}(\mu)}{\varsigma_a}\right)^2 S_\varsigma(\omega)\,d\omega\right)^{1/2} \quad k = 3,4,5, \tag{22}$$

where μ is wave heading (180° for head waves; 0° for following waves). The ITTC wave spectrum was used in the present study:

$$S_\varsigma(\omega) = A\omega^{-5}\exp\left(\frac{-B}{\omega^4}\right) \tag{23}$$

where $A = 173.18H_{1/3}^2/T_{01}^4$ and $B = 692.73/T_{01}^4$ with $H_{1/3}$ significant wave height (m) and T_{01} average wave period (s).

For the calculation of the transfer function of the free-surface elevation due to cushion pressure, the cushion areas are represented by a number of rectangular pressure patches, as in Fig. 2.

The major part of the computation is the calculation of the escape volume in the cushion and the escape area at the leakage openings; this is discussed in Section 3.

3. Free-surface elevation due to oscillatory cushion pressure

In this section, a method is outlined for calculating the free-surface elevation caused by the ALV cushion pressure. The transfer function of the escape area and escape volume in the cushion will be calculated in the frequency domain. The cushion area is

Please cite this article as: Xie, N., et al., A seakeeping analysis method for an air-lifted vessel. Ocean Engineering (2008), doi:10.1016/j.oceaneng.2008.06.011

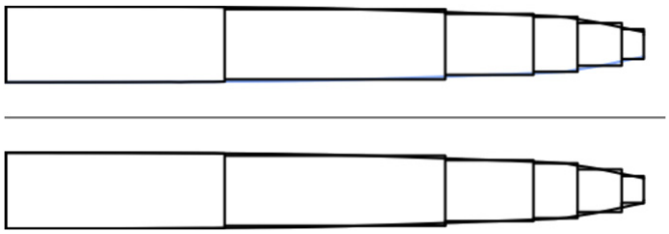

Fig. 2. Representation of the cushion areas of the ALV.

modelled by rectangular pressure patches. The solution for a rectangular pressure patch provides the elementary solution of the problem. The hydrodynamic boundary value problem for a pressure patch oscillating with constant amplitude and moving on the free-surface of a deep, incompressible, ideal fluid was calculated using the corresponding velocity potential. The free-surface elevation due to a moving oscillating rectangular pressure patch with unit pressure strength can be written as, see, for example, Wehausen and Laitone (1960), Kim and Tsakonas (1981), and Xie et al. (2005):

$$\varsigma_p(x,y) = -\frac{1}{\rho_w g} - \frac{\sum_{m=1}^{8}(-1)^m(J_{0m}+J_{1m}+J_{2m}+J_{3m}+J_{4m}+J_{5m}+J_{6m})}{4\rho_w g\pi^2} \tag{24}$$

Here, ρ_w is the density of water, and

$$J_{0m} = \int_0^{\pi/2} \frac{2}{\sin\theta\cos\theta}\ln|s_m(\theta)|\,d\theta \tag{25}$$

$$J_{1m} = \int_0^{\pi/2} \frac{[E_1(ik_1 s_m) - \pi i(1-\mathrm{sgn}(s_m))]\,e^{ik_1 s_m}}{\sin\theta\cos\theta\sqrt{1+4\tau\cos\theta}}\,d\theta \tag{26}$$

$$J_{2m} = -\int_0^{\pi/2} \frac{[E_1(ik_2 s_m) - \pi i(1-\mathrm{sgn}(s_m))]\,e^{ik_2 s_m}}{\sin\theta\cos\theta\sqrt{1+4\tau\cos\theta}}\,d\theta \tag{27}$$

$$J_{3m} = \int_{\theta_c}^{\pi/2} \frac{E_1(-ik_3 s_m)\,e^{-ik_3 s_m}}{\sin\theta\cos\theta\sqrt{1-4\tau\cos\theta}}\,d\theta - \pi\int_{\theta_c}^{\pi/2} \frac{\sin(k_3 s_m)[1+\mathrm{sgn}(s_m)]}{\sin\theta\cos\theta\sqrt{1-4\tau\cos\theta}}\,d\theta - i\pi\int_{\theta_c}^{\pi/2} \frac{\cos(k_3 s_m)[1+\mathrm{sgn}(s_m)]}{\sin\theta\cos\theta\sqrt{1-4\tau\cos\theta}}\,d\theta \tag{28}$$

$$J_{4m} = -\int_{\theta_c}^{\pi/2} \frac{E_1(-ik_4 s_m)\,e^{-ik_4 s_m}}{\sin\theta\cos\theta\sqrt{1-4\tau\cos\theta}}\,d\theta - \pi\int_{\theta_c}^{\pi/2} \frac{\sin(k_4 s_m)[1-\mathrm{sgn}(s_m)]}{\sin\theta\cos\theta\sqrt{1-4\tau\cos\theta}}\,d\theta - i\pi\int_{\theta_c}^{\pi/2} \frac{\cos(k_4 s_m)[1-\mathrm{sgn}(s_m)]}{\sin\theta\cos\theta\sqrt{1-4\tau\cos\theta}}\,d\theta \tag{29}$$

$$J_{5m} = -i\int_0^{\theta_c} \frac{E_1(-ik_3 s_m)\,e^{-ik_3 s_m}}{\sin\theta\cos\theta\sqrt{4\tau\cos\theta-1}}\,d\theta - \frac{\pi}{2}\int_0^{\theta_c} \frac{e^{k_{3i}s_m}\cos(k_{3r}s_m)[1+\mathrm{sgn}(s_m)]}{\sin\theta\cos\theta\sqrt{4\tau\cos\theta-1}}[1+\mathrm{sgn}(k_{3r})]\,d\theta + \frac{i\pi}{2}\int_0^{\theta_c} \frac{e^{k_{3i}s_m}\sin(k_{3r}s_m)[1+\mathrm{sgn}(s_m)]}{\sin\theta\cos\theta\sqrt{4\tau\cos\theta-1}}[1+\mathrm{sgn}(k_{3r})]\,d\theta \tag{30}$$

$$J_{6m} = i\int_0^{\theta_c} \frac{E_1(-ik_4 s_m)\,e^{-ik_4 s_m}}{\sin\theta\cos\theta\sqrt{4\tau\cos\theta-1}}\,d\theta - \frac{\pi}{2}\int_0^{\theta_c} \frac{e^{k_{4i}s_m}\cos(k_{4r}s_m)[1-\mathrm{sgn}(s_m)]}{\sin\theta\cos\theta\sqrt{4\tau\cos\theta-1}}[1+\mathrm{sgn}(k_{4r})]\,d\theta + \frac{i\pi}{2}\int_0^{\theta_c} \frac{e^{k_{4i}s_m}\sin(k_{4r}s_m)[1-\mathrm{sgn}(s_m)]}{\sin\theta\cos\theta\sqrt{4\tau\cos\theta-1}}[1+\mathrm{sgn}(k_{4r})]\,d\theta \tag{31}$$

Furthermore, $E_1[-ik_l s_m]$ is the exponential integral of complex argument (Abramowitz and Stegun, 1970):

$$E_1(z) = \int_z^{\infty}\frac{e^{-u}}{u}\,du = -\gamma - \log z - \sum_{n=1}^{\infty}\frac{(-1)^n z^n}{n\times n!} \tag{32}$$

where $\gamma = 0.5772\ \ldots$ is Euler's constant.

Finally,

$$\theta_c = \begin{cases} tg^{-1}\left(\frac{1}{4\tau}\right), & \tau > 0.25 \\ 0, & \tau < 0.25 \end{cases} \tag{33}$$

$$s_m(\theta) = \begin{cases} (x-a)\cos\theta + (y-b)\sin\theta, & m=1 \\ (x-a)\cos\theta + (y+b)\sin\theta, & m=2 \\ (x+a)\cos\theta + (y+b)\sin\theta, & m=3 \\ (x+a)\cos\theta + (y-b)\sin\theta, & m=4 \\ (x-a)\cos\theta - (y+b)\sin\theta, & m=5 \\ (x-a)\cos\theta - (y-b)\sin\theta, & m=6 \\ (x+a)\cos\theta - (y-b)\sin\theta, & m=7 \\ (x+a)\cos\theta - (y+b)\sin\theta, & m=8 \end{cases} \tag{34}$$

where a and b are half-length and beam of the rectangular. The four wave numbers are

$$k_1 = \tfrac{1}{2}k_0\sec^2\theta[1+2\tau\cos\theta - \sqrt{1+4\tau\cos\theta}], \tag{35}$$

$$k_2 = \tfrac{1}{2}k_0\sec^2\theta[1+2\tau\cos\theta + \sqrt{1+4\tau\cos\theta}], \tag{36}$$

$$k_3 = \tfrac{1}{2}k_0\sec^2\theta[1-2\tau\cos\theta - \sqrt{1-4\tau\cos\theta}], \tag{37}$$

$$k_4 = \tfrac{1}{2}k_0\sec^2\theta[1-2\tau\cos\theta + \sqrt{1-4\tau\cos\theta}], \tag{38}$$

where $k_0 = (g/U^2)$ is wave number, $\tau = (U\sigma/g)$ is the reduced frequency, and σ is the encounter frequency.

We also note that:

$$\lim_{\theta\to\pi/2}\{k_1\} = k_0\tau^2 = \frac{\sigma^2}{g}, \qquad \lim_{\theta\to\pi/2}\{k_2\} = +\infty, \tag{39}$$

$$\lim_{\theta\to\pi/2}\{k_3\} = k_0\tau^2 = \frac{\sigma^2}{g}, \qquad \lim_{\theta\to\pi/2}\{k_4\} = +\infty. \tag{40}$$

The evaluation of the free-surface elevation (24) is hampered by singularities in the integrand of J_{im}, and by their highly oscillatory behaviour. For example, the integrand of J_{0m} becomes infinite when $\theta\to 0$ and $\theta\to\pi/2$; also $k_2 s_m \to \pm\infty$ as $\theta\to\pi/2$.

To overcome these difficulties, we write $F_m(\theta) = f_m(\theta)/g_m(\theta)$, where $f_m(\theta)$ is regular and $g_m(\theta)$ has a zero of order one at $\theta = \theta_a$. Thus, the integral of $F_m(\theta)$ may be written as

$$I_m = \int_{\theta_a}^{\theta_b}\frac{f_m(\theta)}{g_m(\theta)}\,d\theta = \int_{\theta_a}^{\theta_b}\left[\frac{f_m(\theta)}{g_m(\theta)} - \frac{f_m(\theta_a)}{g'_m(\theta_a)(\theta-\theta_a)}\right]d\theta + \int_{\theta_a}^{\theta_b}\frac{f_m(\theta_a)}{g'_m(\theta_a)(\theta-\theta_a)}\,d\theta. \tag{41}$$

On the right-hand side of (41), we observe that the integrand of the first integral is regular at $\theta = \theta_a$; furthermore, the second integral makes no contribution to the summation in (24). The same approach can be applied to the case when $\theta = \theta_b$. In this way, the singularities in the integrals of the free-surface elevation may be removed.

Please cite this article as: Xie, N., et al., A seakeeping analysis method for an air-lifted vessel. Ocean Engineering (2008), doi:10.1016/j.oceaneng.2008.06.011

In the case of J_{3m}, J_{4m}, J_{5m} and J_{6m}, there is a singularity of order 1/2 at $\theta = \theta_c$ which is integrable:

$$\sqrt{1-4\tau\cos\theta} = \sqrt{\frac{2}{\tau}}\sqrt{\sin\left(\frac{\theta+\theta_c}{2}\right)}\sqrt{\sin\left(\frac{\theta-\theta_c}{2}\right)} \tag{42}$$

when $\theta \in (\theta_c, \pi/2)$, and a direct integration scheme can be used to calculate J_{0m}, J_{1m}, J_{3m} and J_{5m} and J_{6m} in (24).

It then remains to calculate J_{2m} and J_{4m}. Their integrands become highly oscillatory when $\theta \to \pi/2$. Following Xie et al. (2005):

$$u = |\gamma|\frac{\sin\theta}{\cos^2\theta} \tag{43}$$

and where $\gamma = (y-b)/2aF_n^2$ $(m = 1,4,6,7)$, or $\gamma = (x-a)/2aF_n^2$ $(m = 2,3,5,8)$, where $F_n = U/\sqrt{2ag}$ is the Froude number for the element. Thus, the oscillatory behaviour is 'stretched':

$$k_2 s_1 = \psi(\theta)\left[\frac{\sqrt{2\alpha u}}{\sqrt{|\gamma|\sqrt{4u^2+\gamma^2}-\gamma^2}} + \frac{\gamma}{|\gamma|}u\right] \tag{44}$$

where $\alpha = (x-a)/2aF_n^2$, $\psi(\theta) = 0.5(1+2\tau\cos\theta+\sqrt{1+4\tau\cos\theta}$.

Care is also advised when handling the logarithmic singularities in the free-surface elevation integrals (25)–(31).

4. Numerical results

A rectangular pressure patch is selected for validation of the numerical schemes outlined in Section 3. The length-beam ratio of the pressure patch is $a/b = 1$ and patch length Froude number $F_n = 0.50$. The free-surface elevations of the rectangular pressure patch at reduced frequencies of $\tau = 0.2375$ and 0.275 (below and above the critical value of 0.25) are compared with existing results. Due to the phase effect, there are real (Re) and imaginary (Im) parts for the free-surface elevation. The same applies to the escape area and escape volume. Wave-cuts at $y = b$ were compared with those of Doctors (1976), who used a different numerical scheme. The agreement was good (see Figs. 3 and 4).

The non-dimensional free-surface elevation per unit pressure is defined as:

$$\tilde{\varsigma}_p = \rho_w g \varsigma_p. \tag{45}$$

The corresponding non-dimensional escape area and escape volume per unit pressure are

$$\tilde{\alpha} = \frac{\rho_w g \alpha}{L} \tag{46}$$

$$\tilde{v}_p = \frac{\rho_w g v_p}{L^2} \tag{47}$$

Numerical predictions were also carried out for an ALV having principal dimensions as given in Table 1.

The cushion area of the ALV is divided into a number of rectangular elements (see Fig. 2). Some convergence studies have been carried out to find the proper discretisation scheme. Figs. 5 and 6 show real and imaginary part of the non-dimensional free-surface elevation at the cushion longitudinal outer boundary when $F_n = 0.5$, respectively. The free-surface elevation is smooth both in space and reduced frequency due to proper handling of the singularities and the high oscillating behaviour. It can be also observed that the free-surface decrease as the reduced

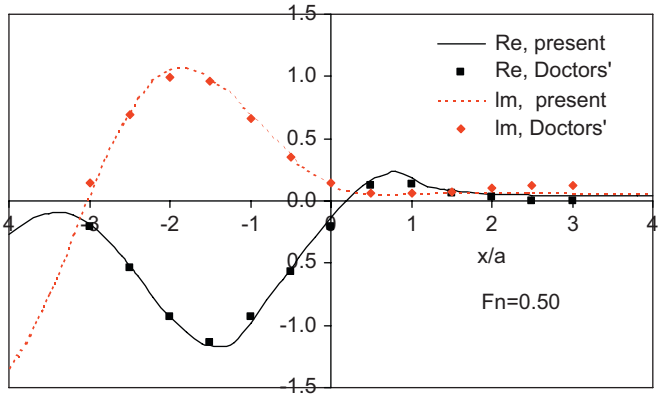

Fig. 3. Non-dimensional free-surface elevation $\tilde{\varsigma}_p$ $y = b$ for a rectangular pressure patch, $b/a = 1$, $\tau = 0.2375$.

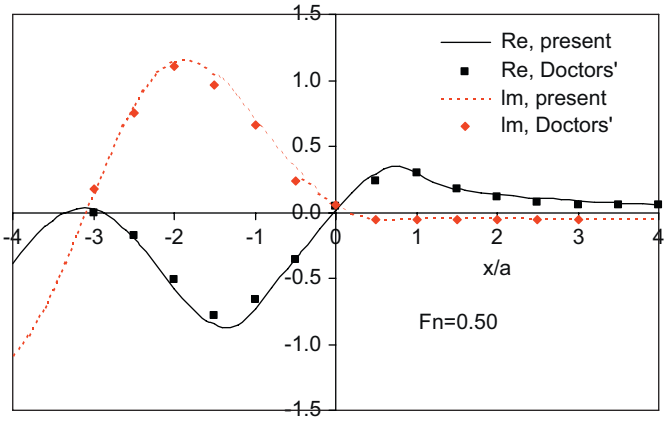

Fig. 4. Non-dimensional free-surface elevation $\tilde{\varsigma}_p$ $y = b$ for a rectangular pressure patch, $b/a = 1$, $\tau = 0.275$.

Table 1
Principal dimensions of the ALV

Length, L_{OA} (m)	40.0
Displacement, Δ (m^3)	170
Breadth, B (m)	15.0
Separation, R (m)	9.60

frequency, τ, increases, which mean that at high (reduced) frequencies, the free-surface elevation responses much less. Figs. 7 and 8 show non-dimensional free-surface elevations at the stern of the ALV when $F_n = 1.0$. The calculated non-dimensional escape areas at the stern opening of the ALV for Froude numbers $F_n = 0.5$, 1.0, 1.5 are shown in Figs. 9–11, respectively. Both demi-hull and twin-hull results are given. In the twin-hull calculation cases, the effect of pressure of one demi-hull on the free-surface elevation of another demi-hull is taken into consideration. It can be seen that the demi-hull has some effect on the escape area of the other demi-hull only for $F_n = 0.5$ and at lower values of frequency. With vessel speed increase, this effect become much less and may be neglected. The escape areas decay quickly with increasing encounter frequency. Also the magnitude of the escape area at lower Froude number is larger than that at higher Froude numbers. Since the craft is normally operating at high speed, this may be probably the reason the craft has good seakeeping

Please cite this article as: Xie, N., et al., A seakeeping analysis method for an air-lifted vessel. Ocean Engineering (2008), doi:10.1016/j.oceaneng.2008.06.011

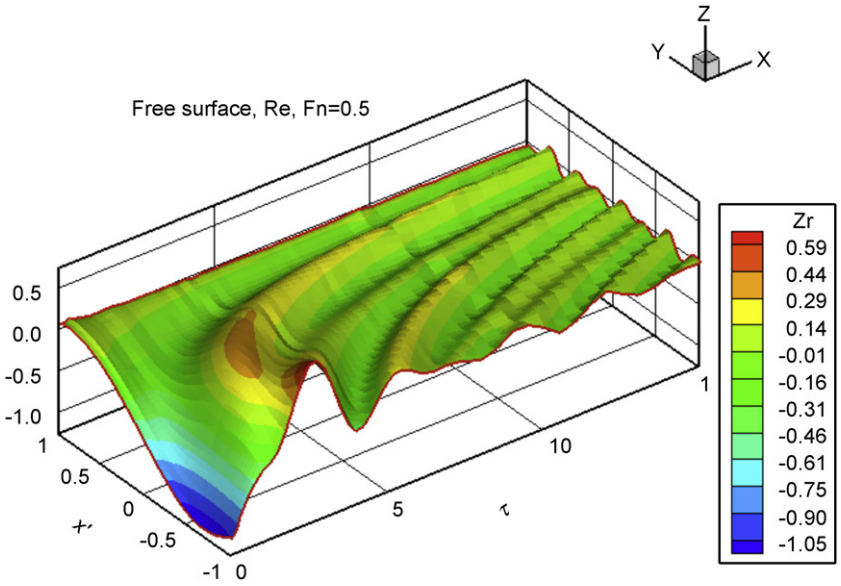

Fig. 5. Real part of $\tilde{\zeta}_p$ at cushion outer boundary of the ALV.

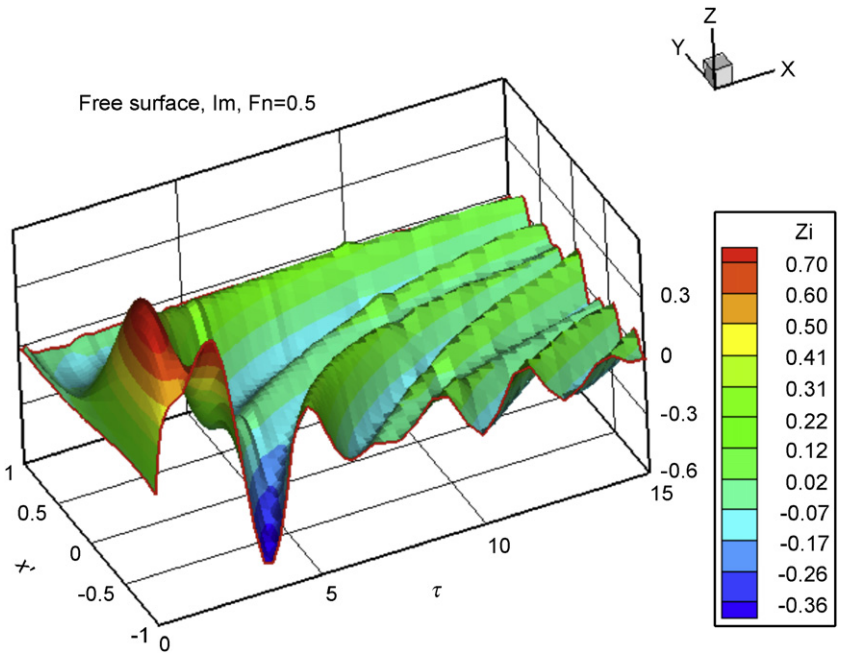

Fig. 6. Imaginary part of $\tilde{\zeta}_p$ at cushion outer boundary of the ALV.

performance. The cushion escape volumes of the ALV for Froude numbers $F_n = 0.5$, 1.0, 2.0 are shown in Figs. 12–14, respectively. The trends are similar to that of the escape area, there will be less free-surface disturbance inside the cushion of the ALV for higher vessel speed.

Using the computed values (46) and (47) in (6) and (20) yields the transfer functions for heave, pitch and roll, from which the spectral responses may be obtained. The RMS of heave, pitch and vertical acceleration on bow of the ALV at $F_n = 1.0$ and four mean wave periods $T_{01} = 4$, 6, 8 and 10 s are plotted in Fig. 15–17, respectively, for all heading angles at interval of 30°. Generally speaking, there will be less craft responses for shorter waves (smaller mean wave periods). Also, the vehicle has less response to head wave than to following seas, this may be due to the characteristics of the free-surface elevation, escape area and escape volume of the cushion of the ALV. At high values of the reduced frequency, the escape area and escape volume both tend to zero: the vessel rides the waves. Figs. 18 and 19 show heave and vertical acceleration at bow of the ALV at $F_n = 1.5$, respectively. Again, the vertical acceleration on bow at following waves is much larger than that at head waves. Although there is no experimental results available for validation of the approach at this stage, the results obtained by the present approach seems reasonable.

Please cite this article as: Xie, N., et al., A seakeeping analysis method for an air-lifted vessel. Ocean Engineering (2008), doi:10.1016/j.oceaneng.2008.06.011

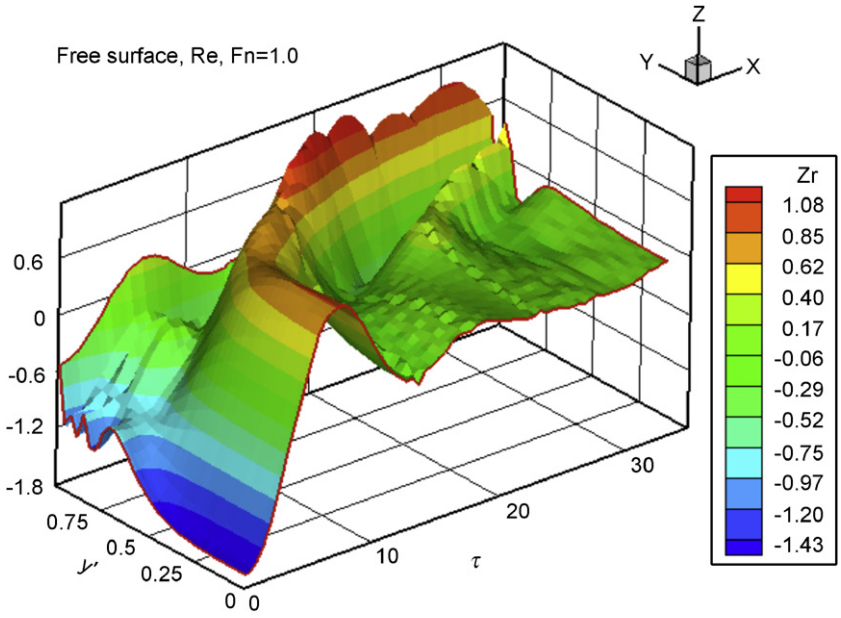

Fig. 7. Real part of $\tilde{\zeta}_p$ at cushion stern boundary of the ALV.

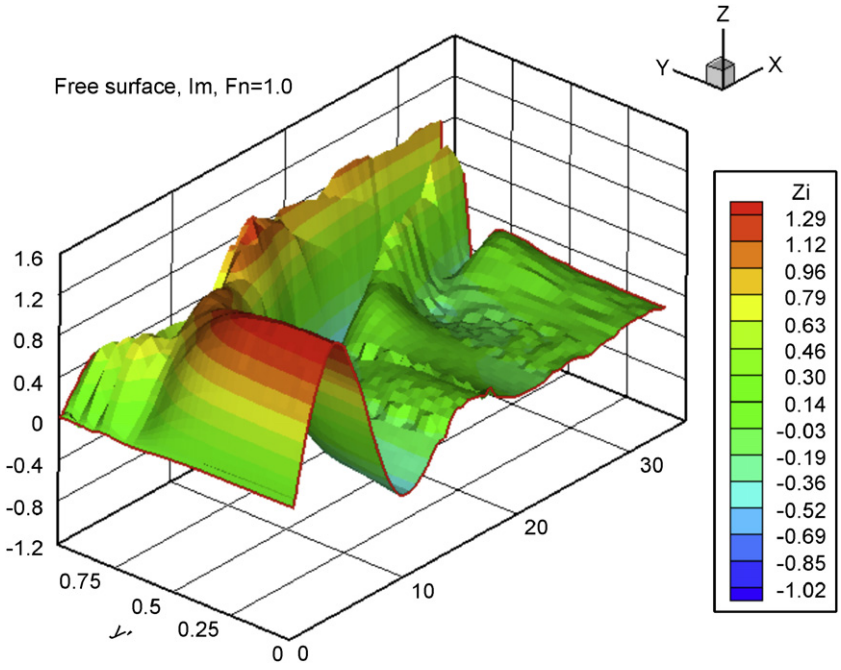

Fig. 8. Imaginary part of $\tilde{\zeta}_p$ at cushion stern boundary of the ALV.

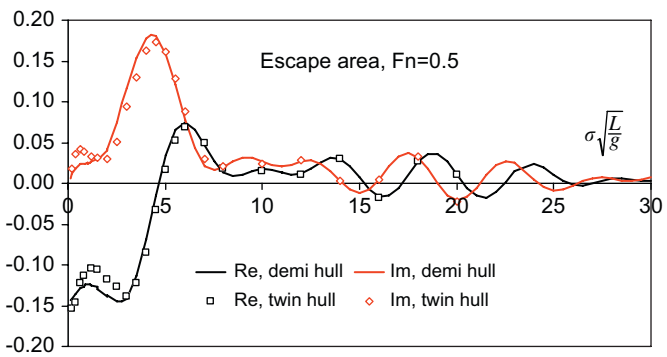

Fig. 9. Non-dimensional escape area $\tilde{\alpha}_p$ at stern of the ALV.

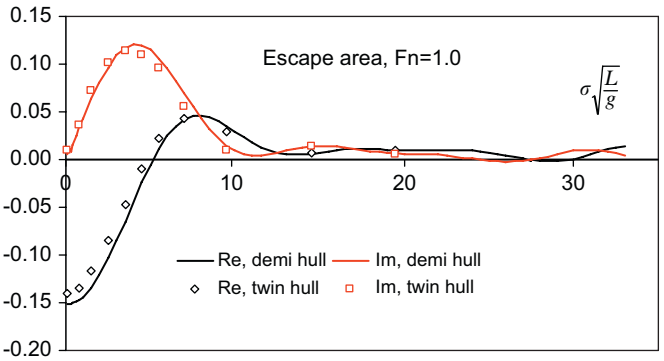

Fig. 10. Non-dimensional escape area $\tilde{\alpha}_p$ at stern of the ALV.

Please cite this article as: Xie, N., et al., A seakeeping analysis method for an air-lifted vessel. Ocean Engineering (2008), doi:10.1016/j.oceaneng.2008.06.011

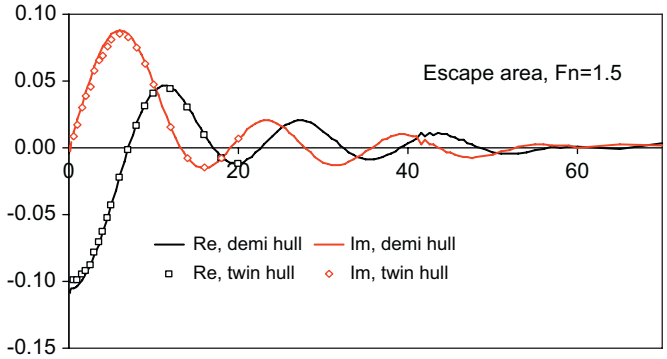

Fig. 11. Non-dimensional escape area $\tilde{\alpha}_p$ at stern of the ALV.

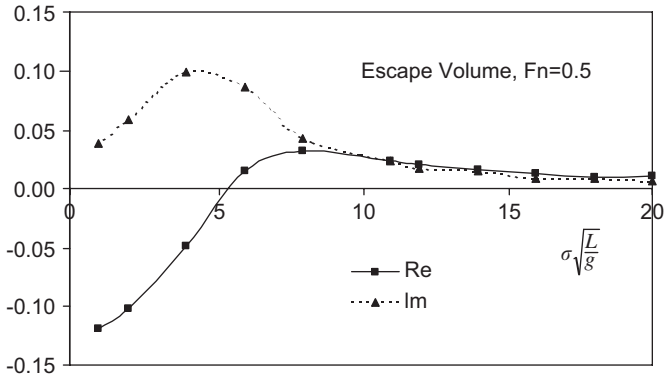

Fig. 12. Non-dimensional escape volume $\tilde{v}_p$ of the ALV.

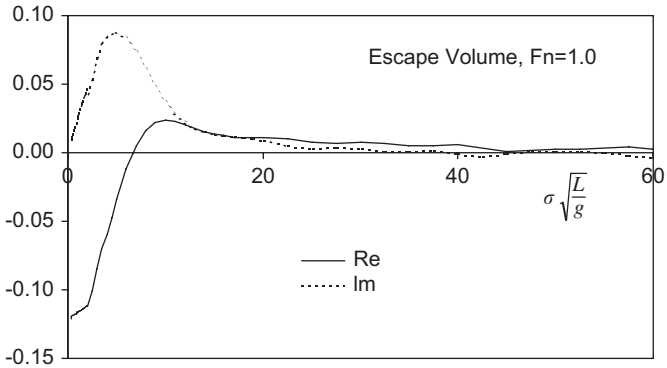

Fig. 13. Non-dimensional escape volume $\tilde{v}_p$ of the ALV.

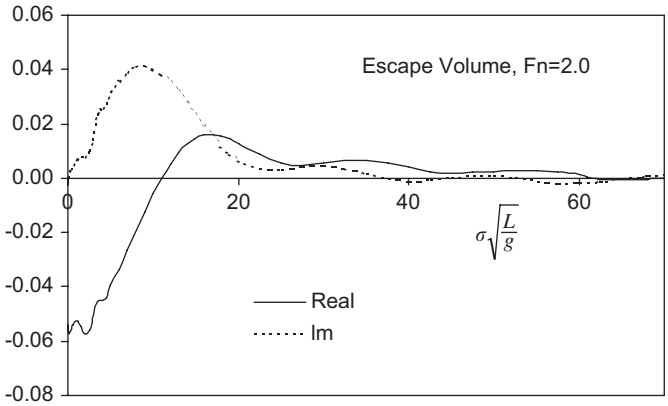

Fig. 14. Non-dimensional escape volume $\tilde{v}_p$ of the ALV.

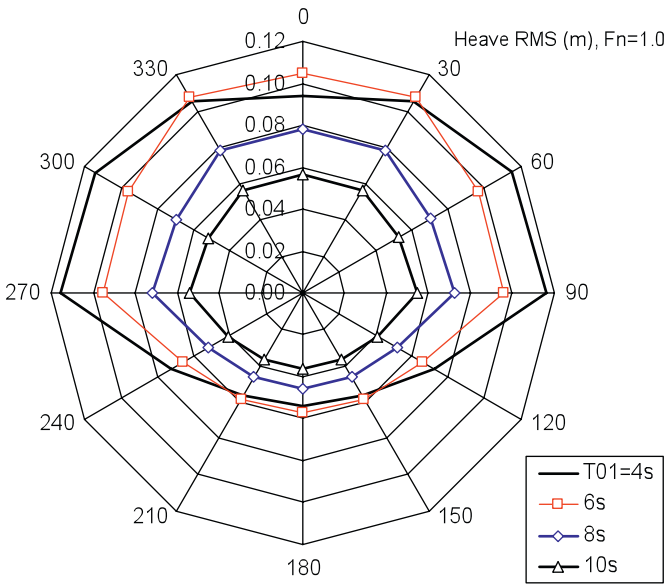

Fig. 15. RMS of heave motion of the ALV at $F_n = 1.0$ for $H_{1/3} = 1$ m.

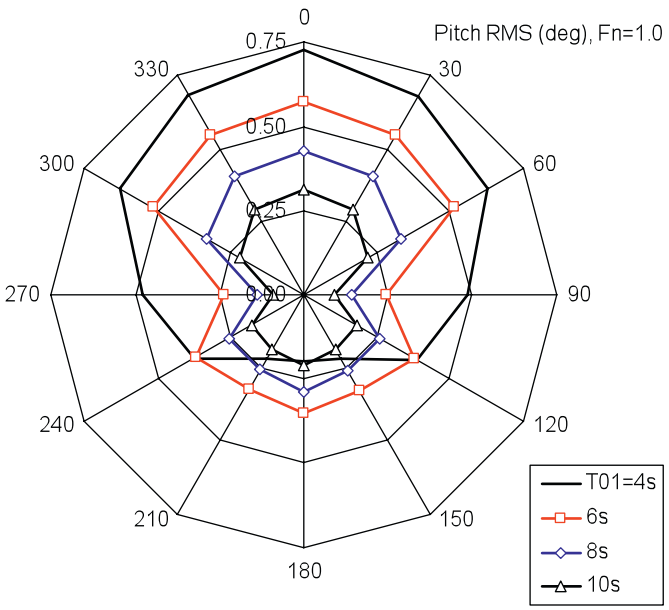

Fig. 16. RMS of pitch motion of the ALV at $F_n = 1.0$ for $H_{1/3} = 1$ m.

5. Conclusions

A mathematical model has been developed to predict the seakeeping performance of an ALV in the frequency domain. The external forces/moments acting on the hull arise from hydrodynamic (added mass and damping) loads, wave excitation—calculated by strip theory—and cushion pressure effects. Attention has focused on the latter: the present method is based on a moving, oscillatory pressure patch. A efficient and effective numerical scheme has been proposed to handle the singularities and highly oscillatory behaviour of several integrands. Results are in good agreement with available published data for the free-surface elevation in the cushion. Numerical results for the escape area, escape volume, and for the vessel motions of the ALV are

Please cite this article as: Xie, N., et al., A seakeeping analysis method for an air-lifted vessel. Ocean Engineering (2008), doi:10.1016/j.oceaneng.2008.06.011

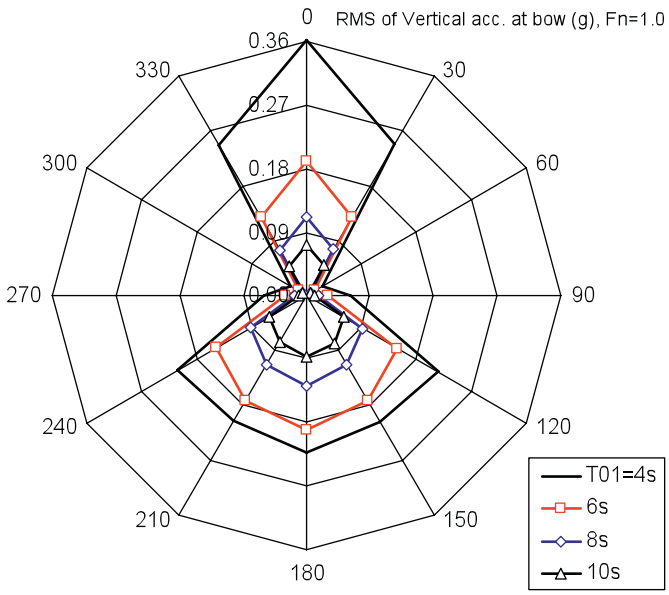

Fig. 17. RMS of vertical acceleration at bow of the ALV at $F_n = 1.0$ for $H_{1/3} = 1$ m.

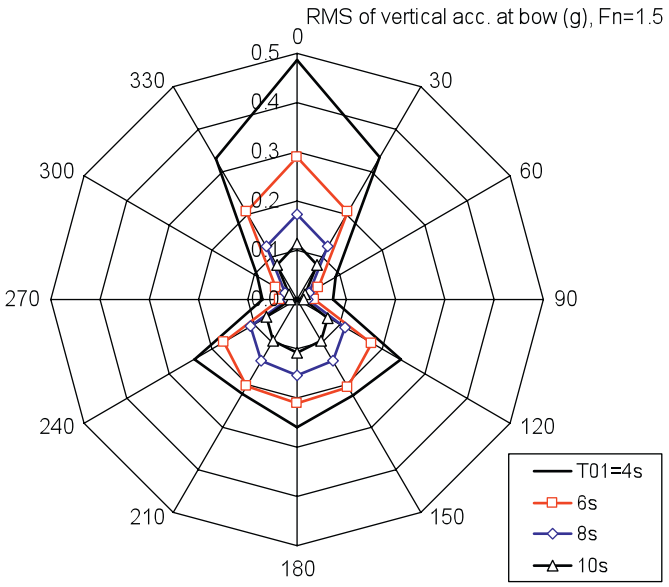

Fig. 19. RMS of vertical acceleration at bow of the ALV at $F_n = 1.5$ for $H_{1/3} = 1$ m.

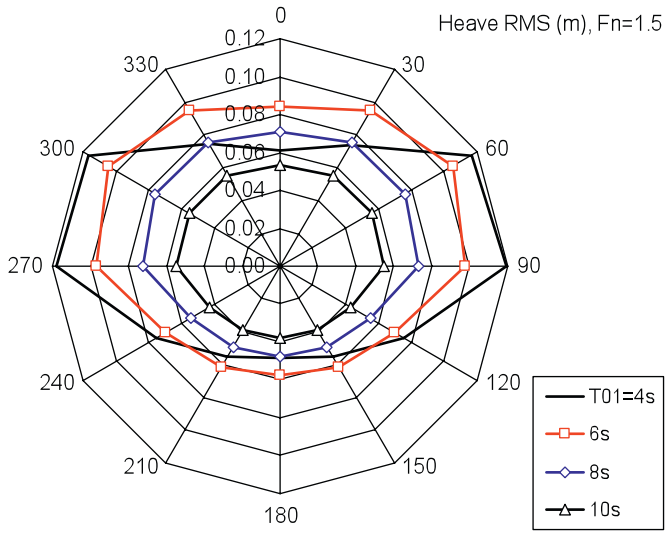

Fig. 18. RMS of heave motion of the ALV at $F_n = 1.5$ for $H_{1/3} = 1$ m.

provided and discussed. The present method therefore appears to provide a helpful means of assessing performance at both design and operational stages.

References

Abramowitz, M., Stegun, I.A., 1970. Handbook of Mathematical Functions. Dover Publications Inc., New York.

Allenstrom, B, Liljenberg, H., Tuden, U., 2001. An Air lifted catamaran. In: Proceedings of the FAST 2001, Southampton, UK.

Allenstrom, B., Liljenberg, H., Tuden, U., 2003. Concept development and model testing—new generation air assisted vessels (AVV) with water jet propulsion. In: Proceedings of the FAST 2003, Naples, Italy.

Chen, H.H., 1977. On a rectangular pressure distribution of oscillating strength moving over a free surface. Journal of Ship Research 21 (1), 11–23.

Doctors, L.J., 1976. The effect of air compressibility on the nonlinear motion of an air-cushion vehicle over waves. In: Proceedings of the 11th ONR Symposium on Naval Hydrodynamics, UCL, London, pp. 373–388.

EFFISES Project, 2001–2004. Energy Efficient Safe Innovative Ships and Vehicle, European Commission CEC Contract no. GRD1-2000-25847, coordinated by SES Europe.

Faltinsen, O.M., 2005. Hydrodynamics of High-Speed Marine Vehicles. Cambridge University Press.

Kaplan, P., Bentson, J., Davis, S., 1981. Dynamics and hydrodynamics of surface effect ships. Transactions of the SNAME 89, 211–247.

Kim, C.H., Tsakonas, S., 1981. An analysis of heave added mass and damping of a surface effect ship. Journal of Ship Research 25 (1).

Wehausen, J.V., Laitone, E.V., 1960. Surface waves in fluid dynamics III. In: Flugge, S., Truesdell, C. (Eds.), Handbuch der Physik, vol. 9. Springer, Berlin, pp. 446–778 (chapter 3).

Xie, N., Vassalos, D., Jasionowski, A., 2005. A study of the hydrodynamics of a three-dimensional planing surface. Ocean Engineering 32, 1539–1555.

Please cite this article as: Xie, N., et al., A seakeeping analysis method for an air-lifted vessel. Ocean Engineering (2008), doi:10.1016/j.oceaneng.2008.06.011